Central-peak—soft-mode coupling in ferroelectric $Gd_2(MoO_4)_3$

J. Petzelt and F. Smutný
Institute of Physics, Czechoslovakian Academy of Sciences, 18200 Prague 8, Na Slovance 2, Czechoslovakia

V. Katkanant, F. G. Ullman, and J. R. Hardy
Department of Physics, University of Nebraska—Lincoln, Lincoln, Nebraska 68588-0111

A. A. Volkov, G. V. Kozlov, and S. P. Lebedev
Institute of General Physics, Academy of Sciences of the Union of Soviet Socialist Republics, 117942 Moscow, Ul. Vavilova 38, Union of Soviet Socialist Republics

(Received 27 December 1983; revised manuscript received 29 June 1984)

Transmission measurements on $Gd_2(MoO_4)_3$ in the (5—50)-cm^{-1} region were performed with use of tunable backward-wave oscillator sources (5—30 cm^{-1}) and a Fourier spectrometer (30—50 cm^{-1}). The resulting dielectric spectra show an additional low-frequency dispersion which was fitted with a standard central-peak model. Its characteristic relaxation frequency is ~ 20 cm^{-1} and the coupling between the soft mode and central mode increases near the transition temperature. This model also accounts very well for the weak anomaly in the clamped permittivity ϵ_c measured at 63 MHz. The same central mode was used to fit earlier Raman soft-mode spectra. All of these data were fitted with a three-coupled-mode model which revealed that the soft-mode spectrum consists of two strongly coupled bare modes: a higher-frequency mode which softens and carries the entire Raman strength and a lower-frequency mode which is hard (59 cm^{-1}) and Raman inactive. Both of these modes are also coupled to the central mode and this coupling increases sharply near the transition. The relatively large width of the central mode indicates its intrinsic nature and suggests partial disorder near the transition.

I. INTRODUCTION

Gadolinium molybdate $Gd_2(MoO_4)_3$ (GMO) is the most studied improper ferroelectric, with a slightly first-order transition at $T_{tr}=432$ K from the high-temperature nonpolar phase [space group $P\bar{4}2_1m(D_{2d}^3), Z=2$] into the improper ferroelectric and improper ferroelastic low-temperature phase [space group $Pba2$ $(C_{2v}^8), Z=4$]. The existence above 640 K of an underdamped soft mode at the M point in the Brillouin zone $[\vec{k}=(\frac{1}{2},\frac{1}{2},0)]$ in isomorphous terbium molybdate (TMO), established by inelastic neutron scattering,[1] gives a strong indication that the transition, at least in TMO, is displacive.

The soft mode fulfills the classical Cochran law $\nu_s^2=1.1(T-T_c)$ cm^{-2} above T_{tr} with $T_c=422$ K and a temperature-independent damping $\Gamma=20\pm4$ cm^{-1}. According to group-theoretical analysis,[2] the soft mode is doubly degenerate above T_{tr}. Below T_{tr} the degeneracy is lifted, and two split, totally symmetric, zone-center, A_1 soft modes are expected in both infrared ($\vec{E}||\vec{c}$) and Raman spectra. Landau-type thermodynamic theory[3,4] requires the frequencies of both soft-mode components ν_{si} $(i=1,2)$ and their splitting $\delta_s=\nu_{s_1}-\nu_{s_2}$ to be proportional to the spontaneous value of the order parameter η_s to first order in $T_{tr}-T$ below T_{tr}, neglecting the discontinuity of the transition. Thus

$$\nu_{si}(T)\propto\delta\nu_s(T)\propto\eta_s(T)\propto[P_s(T)]^{1/2}\ . \tag{1}$$

The last proportionality follows from the improper nature of the ferroelectric transition. The oscillator strengths of both infrared and Raman spectra are similarly given by

$$f_{IR}(T)\propto f_R(T)\propto\eta_s^2(T)\propto P_s(T)\ , \tag{2}$$

where f_{IR} and f_R are proportional to the squares of the soft-mode effective charge and Raman tensor, respectively.

The results of several Raman,[5–16] infrared,[2,17] and neutron scattering[1] investigations are summarized in Fig. 1. One can see that low-temperature Raman measurements have revealed two low-frequency doublets (in the 50- and 80-cm^{-1} regions) which disappear above T_{tr}. Neither pair softens sufficiently to fulfill Eq. (1) (see Fig. 1), but the damping for each increases nonlinearly for $T\rightarrow T_{tr}$. The lower doublet was seen for the first time in far-infrared transmission measurements[17] and was assigned to the soft-mode doublet. The upper doublet is hidden by other stronger lines.

There have been a number of reviews of soft-mode behavior in GMO below T_{tr}; the most recent and thorough are those by Fleury *et al.*[16,18] However, no completely satisfactory explanation of the anomalous behavior of frequency and damping has emerged.

A possible explanation could be provided if the existence of an additional low-frequency central mode that is coupled to the higher-frequency modes could be established. However, it is also known from thorough investigations of the acoustic modes (Yao *et al.*[19] and references

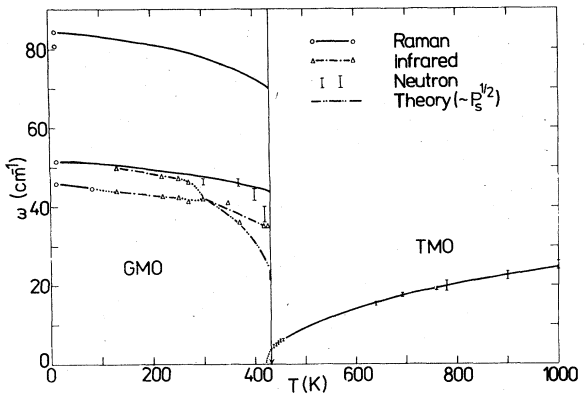

FIG. 1. Summary of soft-mode behavior in GMO (below T_{tr}) and TMO (above T_{tr}). The theoretical curve proportional to $(P_s)^{1/2}$ neglects the soft-mode splitting and fits the infrared data at 300 K.

therein; Fleury *et al.*[16]) that there are marked anomalies in the elastic constants at T_{tr}. The most pronounced is that in C_{11}, which shows no dispersion in the region between 10^7—2×10^{10} Hz ($\nu<1$ cm^{-1}). Associated with this elastic anomaly is an anomalous increase in the damping of the corresponding longitudinal acoustic modes. These anomalies apparently imply that a large decrease in the soft-mode frequency is required.

To justify this proposed explanation of the phase transition, the central mode must be observed experimentally and a theoretical model, that includes this mode, and can provide a unified explanation of all existing Raman, infrared, and elastic data needs to be developed. The existence of a central peak has now been established by transmission measurements in the (3—50)-cm^{-1} region, described in the next section, which clearly reveal a weak additional dielectric dispersion with all the characteristics of a central peak. In addition, a central mode in the 10-cm^{-1} region was recently observed by Siny and coworkers[14,15] in high-resolution Raman scattering. The remainder of this paper is devoted to developing a new phenomenological model which provides a unified understanding of existing data and in which the central mode plays a crucial role.

II. EXPERIMENTAL RESULTS

The transmission measurements were performed on samples polished into plane-parallel plates containing the tetragonal c axis with the electric field $\vec{E}\|\vec{c}$. Measurements in the (3—30)-cm^{-1} region were made with the monochromatic backward wave oscillator (BWO) spectrometer[20] at the former Physical Institute, Moscow, and in the (15—50)-cm^{-1} region on a Beckman LR100 Fourier lamellar-grating interferometer with a Golay detector at the Institute of Physics, Prague. The spectral region 3—30 cm^{-1} is covered by five BWO's, each of which is continuously tuned by an applied dc voltage which can vary the radiation frequency by a factor of up to two. In this way a high-power (1—10 mW) and highly monochromatic ($\Delta\nu/\nu\sim10^{-5}$) source is obtained which permits very precise measurements in the (3—30)-cm^{-1} region.

For the measurements with the BWO spectrometer, we used a plate 3.11 mm thick and about 2 cm^2 in area. For the measurements with the LR100, we divided this sample further into three plates, 0.55 mm thick after polishing, and prepared a mosaic of them. The resulting transmittance spectra at 300 K are shown in Fig. 2. Also shown is the low-frequency spectrum at 422 K near T_{tr}, where the sample is most opaque. More detailed transmittance data in the narrow spectral region 19—22 cm^{-1} indicated in Fig. 2, where the effects of temperature are greatest, are shown in Fig. 3; these are actual spectra taken with one specific BWO.

In most cases, pronounced multiple-reflection interference spectra are seen. Then, the transmittance measurements alone are sufficient for the evaluation of both of the optical constants, n and k (the complex index of refraction is $n^*=n-ik$), and finally of the complex dielectric function $\epsilon^*=\epsilon'-i\epsilon''$ ($\epsilon'=n^2-k^2$, $\epsilon''=2nk$). The values of the refractive index $n(\nu_m)$ at the interference maxima, ν_m, are obtained from

$$n(\nu_m)=\frac{m}{2\nu_m d},\quad m=1,2,\ldots, \tag{3}$$

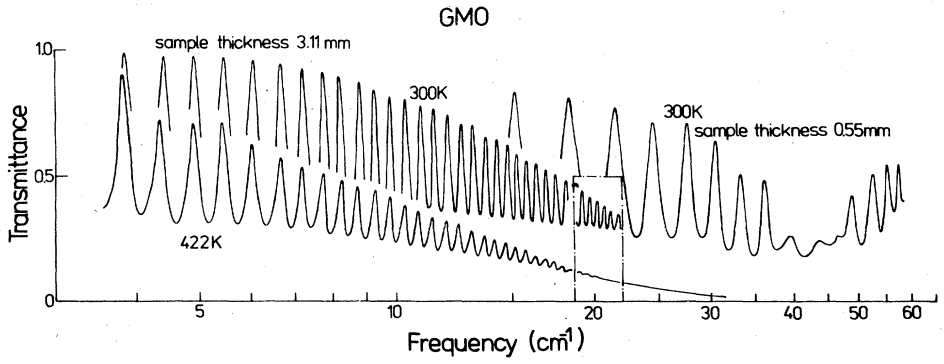

FIG. 2. Transmittance spectra of GMO: an illustration.

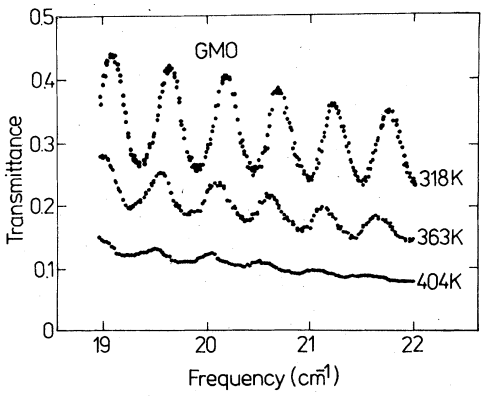

FIG. 3. Transmittance spectra using one BWO: measured output from the spectrometer.

where d is the sample thickness. Then the absorption index $k(\nu_m)$ for $k \ll n$ can be calculated iteratively from the approximate equation for the transmittance,

$$\mathcal{T}(\nu_m) \simeq \frac{(1-R)^2}{e^{\alpha d}+R^2 e^{-\alpha d}-2R} , \tag{4}$$

where the absorption coefficient is $\alpha = 4\pi\nu k$ and the normal bulk reflectivity is

$$R = \frac{(n-1)^2+k^2}{(n+1)^2+k^2} . \tag{5}$$

When the condition $k \ll n$ is not satisfied, it is better to determine both optical constants iteratively from $\mathcal{T}(\nu)$ using the rigorous formula[20]

$$\mathcal{T}(\nu) = \frac{(1-R)^2+4R\sin^2\theta}{e^{\alpha d}+R^2 e^{-\alpha d}-2R\cos[2(\phi+\theta)]} , \tag{6}$$

where

$$\theta = \tan^{-1}\frac{2k}{n^2+k^2-1}$$

and (7)

$$\phi = 2\pi\nu n d .$$

In the few cases where no interference peaks are seen, independent measurements of the phase spectrum $\Phi(\nu)$ of the transmitted wave were performed using a two-beam Mach-Zehnder (Rozhdestvensky) polarizing interferometer. The increase Δl of the optical path due to the presence of the sample, which is measured using the compensation method, is

$$\Delta l(\nu) = \frac{\Phi(\nu)}{2\pi\nu} - d , \tag{8}$$

where

$$\Phi(\nu) = \phi - \tan^{-1}\frac{(n^2+k^2-1)k}{(n^2+k^2)(n+2)+n} + \tan^{-1}\frac{\mathrm{Re}^{-\alpha d}\sin[2(\phi+\theta)]}{1-\mathrm{Re}^{-\alpha d}\cos[2(\phi+\theta)]} . \tag{9}$$

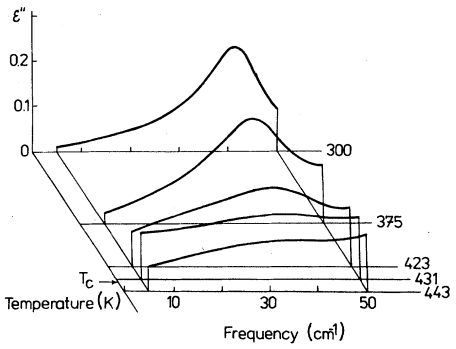

FIG. 4. Dielectric-loss spectra of GMO.

The optical constants are then calculated directly from Eqs. (6) and (9) independently for each ν.

The results for the imaginary part of the permittivity $\epsilon''(\nu)$ are shown in Fig. 4. We omitted data in the (3–5)-cm^{-1} region because these were influenced by an instrumental error due to finite sample size. The real part of the permittivity ϵ' equals 8.7 and is independent of frequency for $\nu < 30$ cm^{-1} at 300 K. Interferometric measurements of $\Phi(\nu, T)$ permitted a determination of the relative variation of $\epsilon'(T)$ with a precision of $\pm 10^{-3}$. With increasing temperature, ϵ' increases by ~ 0.1 and, near T_{tr}, a distinct downward step of about 0.05 is observed. This step appears sharper the lower the frequency used, but its total magnitude is frequency independent for $\nu < 30$ cm^{-1}. An even more pronounced and sharper downward step is observed in the $\epsilon''(T)$ curves at T_{tr}. The magnitude of this step increases as ν decreases, as is shown in Fig. 5.

To check the anomaly in ϵ' more closely, we performed clamped permittivity measurements at 63 MHz. A model B801 Wayne-Kerr V.H.F. admittance bridge was provided with a pair of flat, sandwich-like, rugged, stainless-steel leads, pointing upwards and connecting directly to the bridge terminals with the sample in a bottom-loaded variable-temperature chamber. The measuring signal was modulated by a 1223-Hz square wave and the audio-frequency detector was a Keithley model 192 DMM. The samples were circular slabs, 8 mm in diameter and ~ 0.1 mm in thickness in a direction perpendicular to the c axis. Evaporated aluminum electrodes were used. The variation of sample dimensions with temperature was taken

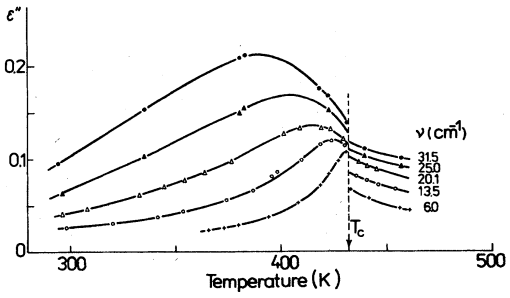

FIG. 5. Temperature dependence of the dielectric losses for several fixed frequencies.

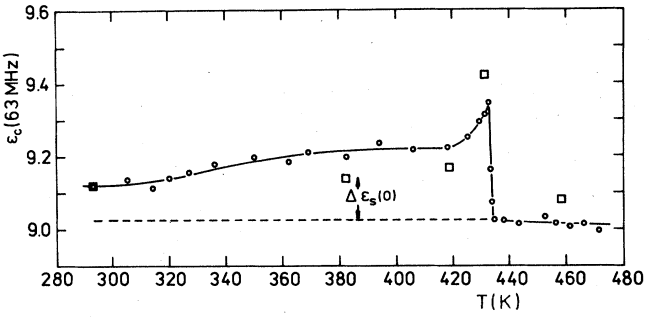

FIG. 6. Temperature dependence of the clamped permittivity ϵ_c at 63 MHz; 9 V/cm (circles). Calculated values according to Eq. (20) (squares).

into account using the thermal-expansion data published by Cummins.[21] The resulting temperature dependence of ϵ_c is shown in Fig. 6. Although the samples were probably multidomain, the close similarity between $\epsilon_c(T)$ at 5 cm^{-1} and at 63 MHz suggests that the dispersion due to domain walls is of minor importance above 63 MHz. The absolute error of ϵ_c due to the uncertainty in determining the sample geometry and stray capacitance effects, as well as the reproducibility with different samples, did not exceed $\pm 1.3\%$. This error, however, does not influence the shape of the anomaly near T_{tr}.

A. Infrared spectra

Earlier infrared measurements[17] above 20 cm^{-1} were taken only up to 350 K. A comparison of those taken at 300 K with the present data, shown in Fig. 4, shows good agreement. However, the present data have a lower background absorption. In Fig. 4 the peak in $\epsilon''(\nu)$ can be seen to remain at finite frequency (~ 30 cm^{-1}) as T_{tr} is approached. The theoretical dependence of ν_s on T, derived from Eq. (1), is shown in Fig. 1 together with various experimental data. There is a clear disagreement, in that the theoretical results show too large a softening. However, Figs. 4 and 5 show that at low frequencies $\epsilon''(\nu)$ increases markedly as T_{tr} is approached. This is clear evidence for additional low-frequency absorption. This can be made more visible by plotting the spectral function or dynamical structure factor, $S(\nu) \propto T\epsilon''(\nu)/\nu$ rather than $\epsilon''(\nu)$.

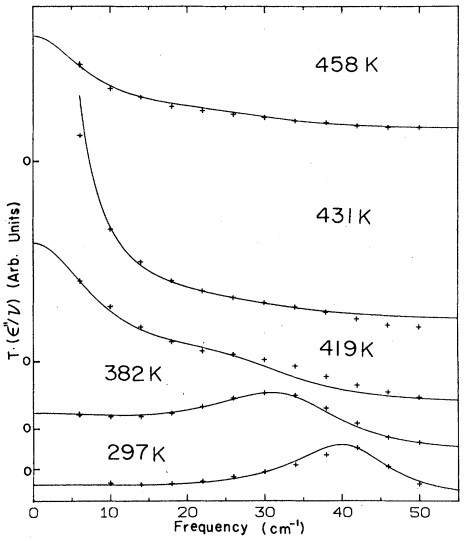

FIG. 7. $T\epsilon''(\nu)/\nu$ spectra showing the central mode behavior together with their fit using Eq. (11) with parameters listed in Table I.

This quantity, which is proportional to the Raman scattering intensity, is shown in Fig. 7. Clear central-peak behavior is seen near but below T_{tr}. Above T_{tr}, a qualitatively similar but weaker central peak remains.

Neglecting the soft-mode splitting, we attempted to fit the spectra in Fig. 7 to the response of an oscillator coupled to a Debye relaxation, a model which is frequently used for the description of central-peak behavior.[22] This response is given by

$$\Delta\epsilon_s(\nu) = \frac{f_{IR}(T)}{\nu_{IR}^2(T) - \nu^2 + i\Gamma\nu - \delta^2/(1+2\pi i\nu\tau)} , \tag{10}$$

where f_{IR}, ν_{IR}, and Γ are the oscillator strength, eigenfrequency, and damping of the bare soft-mode oscillator, respectively, and δ is the real coupling constant for coupling between the oscillator and the Debye relaxation with a bare relaxation frequency $(2\pi\tau)^{-1}$.

The structure factor is then given by

$$S(\nu) \propto \frac{T\epsilon''(\nu)}{\nu} = \frac{Tf_{IR}(T)\left[\Gamma + \dfrac{\tau\delta^2}{1+4\pi^2\nu^2\tau^2}\right]}{\left[\nu_{IR}^2 - \dfrac{\delta^2}{1+4\pi^2\nu^2\tau^2} - \nu^2\right]^2 + \left[\Gamma + \dfrac{\tau\delta^2}{1+4\pi^2\nu^2\tau^2}\right]^2\nu^2} + a . \tag{11}$$

The additional constant a in Eq. (11) accounts for a background absorption due to all higher-frequency oscillators. The frequency ν_{IR} represents the mean frequency of the bare soft-mode doublet. This model assumes that the oscillator strength of the bare relaxation (i.e., central mode) is zero. Thus, the central mode appears only through its coupling to the soft-mode whose oscillator strength is f_{IR}. It is obvious that it would be meaningless to fit each measured spectrum to Eq. (11), allowing all six parameters to vary independently. Thus their number was reduced by several physically reasonable assumptions. First, we assumed that the strength $f_{IR}(T)$ is proportional to P_s [Eq.

TABLE I. Parameters of the infrared fit shown in Fig. 7 using Eq. (11).

$T(K)$	ν_{IR} (cm^{-1})	Γ (cm^{-1})	f_{IR} (cm^{-2})	$(2\pi\tau)^{-1}$ (cm^{-1})	δ (cm^{-1})	a	Ω_{IR} (cm^{-1})
297	41.7	13	150	20	14.6	0.1	39
382	35	17	113	20	15.7	0.6	31.3
419	30	18	68	20	21	0.9	21.4
431	28.7	19	38	20	27	1.4	10
458	28.7	20	24	20	21	1.1	20

(2)] as required by thermodynamic theory (the P_s data were taken from work by Cummins[21]). Second, we assumed the bare frequency ν_{IR}^2 to be given by

$$\nu_{IR}^2 = A_{IR}(T - T_{IR}) , \tag{12}$$

where T_{IR} is a parameter whose only constraint is that it be compatible with our fit to the Raman data, to be described later. Third, we assumed τ to be temperature independent. The fourth and final condition, required of any reasonable fit, involves the critical temperature T_c', at which the low-temperature phase becomes absolutely unstable. T_c' should lie very close to but above T_{tr} to be compatible with static experiments and with acoustic data. The latter show no dispersion up to about 20 GHz, which implies that the piezoelectric coupling does not influence T_c', in agreement with the fact that the corresponding piezoelectric constant d_{31} must go to zero at T_c'. To demonstrate that our model predicts an instability at T_c', the temperature dependence of the inverse soft-mode static susceptibility should be calculated. This quantity is proportional to the square of the effective soft-mode frequency,

$$\Omega_{IR}^2 = \nu_{IR}^2 - \delta^2 \tag{13}$$

which is probed by experiments at $\nu \ll \Omega_{IR}$ [see Eq. (10)]. We have shown in the fitting of the infrared data to this model that an Ω_{IR}^2 that goes to zero just above T_{tr} is in fact obtained. The resulting fitted spectra are shown in Fig. 7. While the fits appear worse at the high-frequency end, this discrepancy is of little importance since the experimental accuracy is lower in this region due to the limitations of the Fourier-transform technique. We also included in the fitting the multiphonon spectrum above T_{tr} at 458 K. The resulting parameters have no clear physical meaning but provide a means for estimating this background absorption.

The fitted parameters at each temperature, together with the effective frequency Ω_{IR}, are shown in Table I. The bare soft-mode frequency is given by Eq. (12) with $A_{IR} = 6.9\ cm^2 K^{-1}$ and T_{IR} (which is the instability temperature in the absence of the central mode) is approximately 550 K. The fit is not very sensitive to the central-peak relaxation frequency $(2\pi\tau)^{-1}$: Any value between 20 and 25 cm^{-1} is satisfactory. However, our subsequent fit to the Raman data requires that $(2\pi\tau)^{-1}$ not be greater than 20 cm^{-1}. The most important result is the marked increase of δ near T_{tr}. All fits with a temperature-independent δ failed, because $\delta \approx 27\ cm^{-1}$ in order to bring T_c' close to T_{tr}, and this is much too high to fit the low-temperature spectra. Thus one can see that the shift of the instability temperature $T_{IR} \approx 550$ K down to $T_c' = 435$ K is caused by a coupling between the soft mode and the central mode which increases nonlinearly with temperature close to T_{tr}.

B. Raman spectra

As a basis for the Raman fit, we used data taken earlier.[12] They were taken in the $x(zz)y$ geometry where both anomalous modes in the 40- and 80-cm^{-1} regions are

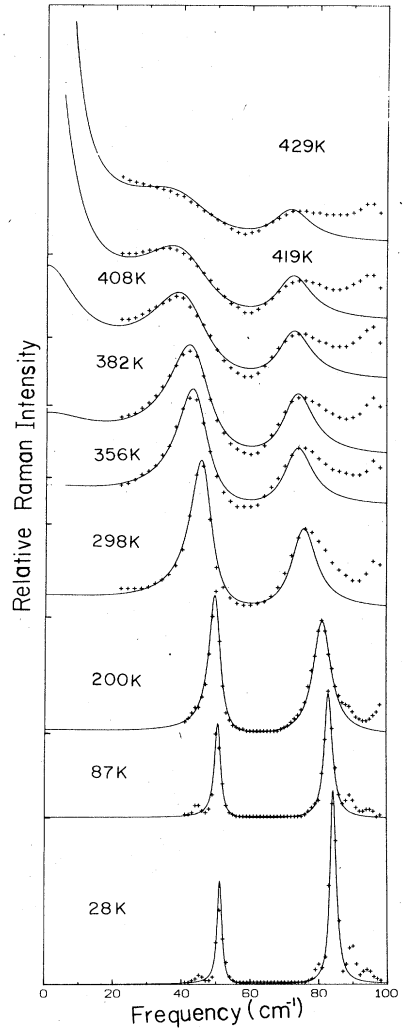

FIG. 8. Some of the $x(zz)y$ Raman soft-mode spectra and their fit using Eq. (14) with parameters listed in Table II. The crosses represent the experimental data, full lines are the theoretical fit.

the strongest. Some of the spectra are shown in Fig. 8. The anomalous behavior of both modes as functions of both temperature and uniaxial stress was reported in Ref. 12 and in earlier references quoted therein. No theoretical fit was attempted in this early work because there was no evidence of the existence of a central mode and the soft-mode behavior was not understood. However, some basic facts, already alluded to, were established; both modes split into doublets at low temperature and both disappear above T_{tr}. Therefore, each mode belongs to a doubly degenerate M-point mode of T_1 symmetry in the parent phase. Since this is also the symmetry of the order parameter, it would appear that one of the doublets has to be the soft-mode doublet (according to group theory,[2] we can expect six external mode doublets of T_1 symmetry to appear in both infrared and Raman spectra below T_{tr}).

Obviously, the upper and lower Raman doublets are strongly coupled and a definite intensity transfer from the lower-frequency doublet Q_2 to the higher frequency doublet Q_1 can be seen as T decreases. This led us to the assumption that, far below T_{tr}, the Q_1 doublet represents predominantly the soft-mode doublet which has greater strength, while close to T_{tr} both modes become involved in the phase transition. Therefore, to analyze the Raman spectra properly, we have to consider both doublets and the central mode Q_3. Fortunately, we can safely neglect the lower-frequency components of each doublet since they are much weaker and are not resolved above 300 K.

Thus we are left with a three coupled-mode problem for which the susceptibility is given by

$$\chi(\nu)=\frac{\epsilon_1\begin{vmatrix}\epsilon_1 & \delta'_{12} & \delta'_{13}\\ \epsilon_2 & \nu_2^2-\nu^2+i\nu\Gamma_2 & \delta'_{23}\\ 0 & \delta'_{23}/2\pi\Gamma_3 & (2\pi\tau)^{-1}+i\nu\end{vmatrix}+\epsilon_2\begin{vmatrix}\nu_1^2-\nu^2+i\nu\Gamma_1 & \epsilon_1 & \delta'_{13}\\ \delta'_{12} & \epsilon_2 & \delta'_{23}\\ \delta'_{13}/2\pi\Gamma_3 & 0 & (2\pi\tau)^{-1}+i\nu\end{vmatrix}}{\chi(\nu)=\begin{vmatrix}\nu_1^2-\nu^2+i\nu\Gamma_1 & \delta'_{12} & \delta'_{13}\\ \delta'_{12} & \nu_2^2-\nu^2+i\nu\Gamma_2 & \delta'_{23}\\ \delta'_{13}/2\pi\Gamma_3 & \delta'_{23}/2\pi\Gamma_3 & (2\pi\tau)^{-1}+i\nu\end{vmatrix}} \quad (14)$$

Here ν_i, ϵ_i, and Γ_i are the eigenfrequency, Raman tensor, and damping, respectively, of the mode Q_i, and δ'_{ij} is the coupling constant between the modes Q_i and Q_j. The Stokes Raman spectrum is then given by

$$S(\nu)=-\left\{\left[\exp\left[\frac{h\nu}{k_BT}\right]-1\right]^{-1}+1\right\}\mathrm{Im}\chi(\nu)+b\ , \quad (15)$$

where again the constant base line b accounts for all higher-frequency modes.

In general, the coupling constants δ'_{ij} can be complex; however, we are seeking the simplest possible description of our system: Specifically, we wish to isolate, in a physically meaningful way, the basic temperature dependences that drive the transition. If this can be achieved using real δ'_{ij}'s, then these are the most convenient.

An initial trial and error fit using formulas (14) and (15) showed that the best fit could be obtained by taking $\epsilon_2=0$, $\delta'_{12}\sim 1750\ \mathrm{cm}^{-2}$, and $\nu_2=59\ \mathrm{cm}^{-1}$, independent of temperature. The first condition means that the strength of the whole spectrum below 90 cm^{-1} is determined by the Q_1 mode alone, which is also the only temperature-dependent mode. In this situation, Eq. (14) reduces to

$$\chi(\nu)=f_R[(\nu_2^2-\nu^2+i\nu\Gamma_2)(\nu_3+i\nu)-\delta_{23}^2]\times\{(\nu_1^2-\nu^2+i\nu\Gamma_1)[(\nu_2^2-\nu^2+i\nu\Gamma_2)(\nu_3+i\nu)-\delta_{23}^2]-\delta_{12}^2(\nu_3+i\nu)-\delta_{13}^2(\nu_2^2-\nu^2+i\nu\Gamma_2)+2\delta_{12}\delta_{13}\delta_{23}\}^{-1}\ , \quad (16)$$

where

$$\delta_{12}=\delta'_{12},\ \ \delta_{13}=\delta'_{13}/(2\pi\Gamma_3)^{1/2},\ \ \delta_{23}=\delta'_{23}/(2\pi\Gamma_3)^{1/2}\ ,$$

the Raman strength $f_R=\epsilon_1$, and $\nu_3=(2\pi\tau)^{-1}$ is the central-mode relaxation frequency. Γ_3 is the overcritical damping of the central mode, which is equal to the reciprocal kinetic coefficient and is generally assumed to be temperature independent in the mean field approximation. In our fit we assumed that $\nu_3=20\ \mathrm{cm}^{-1}$ and is independent of T. This is consistent with our infrared data, but we also found that the Raman data were much more sensitive to the value of ν_3 for $\nu_3>20\ \mathrm{cm}^{-1}$ and it is therefore effectively fixed by the Raman fits. The coupling constants to the central peak δ_{13} and δ_{23} have to fulfill the requirement that the system becomes unstable at $T_c'=435$ K, as was the case for the infrared response. Therefore we also examined the behavior of the effective soft-mode frequency probed by low-frequency experiments, such as Brillouin scattering, or ultrasonic propagation. For our model, this frequency Ω_R is given by

$$\Omega_R^2\equiv\frac{f_R}{\chi(0)}=\frac{\nu_1^2\nu_2^2\nu_3-\nu_1^2\delta_{23}^2-\nu_2^2\delta_{13}^2-\nu_3\delta_{12}^2+2\delta_{12}\delta_{13}\delta_{23}}{\nu_2^2\nu_3-\delta_{23}^2} \quad (17)$$

TABLE II. Parameters of the Raman fit (see Fig. 8) using Eqs. (14) and (15). The following parameters are temperature independent: $\nu_2=59\ \mathrm{cm}^{-1}$, $\nu_3=20\ \mathrm{cm}^{-1}$, $\epsilon_2=0$, $\delta_{12}=1750\ \mathrm{cm}^{-2}$, $\delta_{13}=-50\ \mathrm{cm}^{-3/2}$.

T (K)	ν_1 (cm^{-1})	f_R (10^3)	Γ_1 (cm^{-1})	Γ_2 (cm^{-1})	δ_{23} ($\mathrm{cm}^{-3/2}$)	b	Ω_R (cm^{-1})
28	79.2	23.4	2.3	0.5	30	0	72.0
87	77.5	15.4	3.2	0.8	30	0	70.1
111	76.8	18.2	3.8	1.0	30	0	69.3
154	76.4	20.7	5.6	1.3	30	0	68.9
200	75.0	19.0	7.7	1.6	30	0	67.3
251	70.5	19.9	10.2	2.0	30	0	62.3
298	66.3	15.0	12.8	2.5	30	5.4	57.5
323	64.9	13.7	14.0	2.7	30	8.0	55.8
356	63.0	11.5	15.9	3.1	50	10.5	52.9
382	62.9	12.5	17.3	3.4	90	12.1	50.6
408	60.5	10.4	18.7	3.7	130	13.8	43.7
419	60.0	9.8	19.3	3.8	160	9.4	37.1
429	58.4	7.6	19.9	3.9	190	7.4	18.2
431	57.7	7.6	20.0	4.0	193	13.1	11.2

and is required to vanish at ~ 435 K.

Our initial trial-and-error parameters were refined by least-squares fitting. Our aim was to find a monotonic and physically acceptable temperature variation of all parameters. This was achieved by assuming both damping constants Γ_1,Γ_2 to vary linearly with T above ~ 100 K but their T dependence has to level off at low temperatures to values essentially unchanged from the low-temperature values determined in our initial trial fit. The resultant values of Γ_2 are rather small, whereas Γ_1 reaches 20 cm^{-1} at T_{tr}, which is also the value of damping found for the soft mode above T_{tr} from neutron scattering data.[1] The coupling δ_{13} between the Q_1 mode and central mode appears to be roughly T independent and of opposite sign to δ_{12} and/or δ_{23} so that the term $2\delta_{12}\delta_{13}\delta_{23}$ in Eq. (16) is negative (and definitely nonzero). As might be expected, only spectra at temperatures above 300 K are sensitive to the central-mode parameters and couplings δ_{13} and δ_{23}. Therefore we somewhat arbitrarily assumed δ_{13} and δ_{23} to be T independent below 300 K. Close to T_{tr}, however, the fit is very sensitive to δ_{13} and δ_{23} and good results were obtained only by assuming δ_{23} to increase nonlinearly as T approaches T_{tr}. If δ_{23} was fixed at a value sufficiently large to cause Ω_R to vanish at T_c', the central peak would be much too strong at lower temperatures, destroying all agreement between theory and experiment in the low-frequency spectral region.

It is interesting to note in this context that the roles of δ_{13} and δ_{23} are not interchangeable. Increasing δ_{13} results in a strong increase of the central peak, whereas increasing δ_{23} (in such a way as to produce the same Ω_R) results only in a weak central peak. This asymmetry is caused by the fact that the bare Q_2 mode in our model has *zero* Raman strength, so that increasing its coupling to the central peak can produce instability while only weakly enhancing the central peak. This does not contradict the requirement that the integral over the whole spectrum, which is proportional to $\chi(0)$, must diverge at T_c' if f_R remains finite. In the case when δ_{23} dominates, the divergence is simply much weaker than in the case when δ_{13} dominates.

The resulting fitted parameters are shown in Table II and some of the fitted spectra in Fig. 8. The spectra between 28 and 251 K were fitted in the region 40—90 cm^{-1} and the additional weak peaks near 45, 80, and 90 cm^{-1} were neglected during the fit. The spectra from 298 to 431 K were fitted in the (20—80)-cm^{-1} region. The weak scatter in the Raman strength f_R is most probably caused by fluctuations in the laser power, which was not stabilized during the experiment (performed in 1976). Theoretically, one would expect this parameter to follow $P_s(T)$ [see Eq. (2)] which would imply a decrease by a factor of 4 between 298 K and T_{tr} which is somewhat more than what is observed.

The quality of the fits is satisfactory, except at the high-frequency ends, where obviously other modes are present. The only slight systematic deviation outside the limits of experimental error seems to occur in the region of the deep minimum at $\sim 60\ \mathrm{cm}^{-1}$ between both peaks. Also at higher temperatures the overall quality of the fit is slightly worse.

IV. DISCUSSION

Let us first compare the results of the infrared and Raman fits. First, it is to be stressed that the basic difference between the infrared and Raman models is only due to the different spectral and temperature regions involved in the fit. In Fig. 9 the squares of all relevant frequencies are plotted against temperature. The observed Raman frequency ν_- is slightly higher than that of the corresponding infrared peak because in Raman scattering we see (for $T \gtrsim 300$ K) only the higher-frequency component of the doublet, whereas in the infrared both components occur with comparable strengths but cannot be resolved above room temperature. The Q_1 mode was not seen in our infrared transmission experiment[17] because the absorption above 70 cm^{-1} was too great. From Fig. 9 we see that the dependence of ν_1^2 on T is almost linear above ~ 200 K, reaching instability ($\nu_1=0$) at ~ 850 K. This would be the transition temperature if no coupling with Q_2 and the

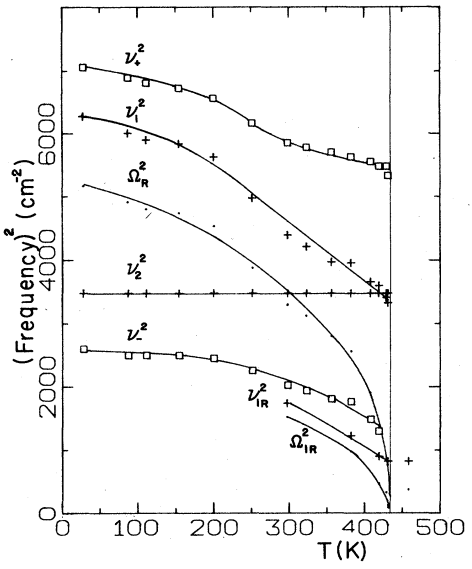

FIG. 9. Temperature dependence of the squares of various mode frequencies. ν_+ and ν_- are the experimental Raman peak positions; the meaning of other symbols is explained in the text.

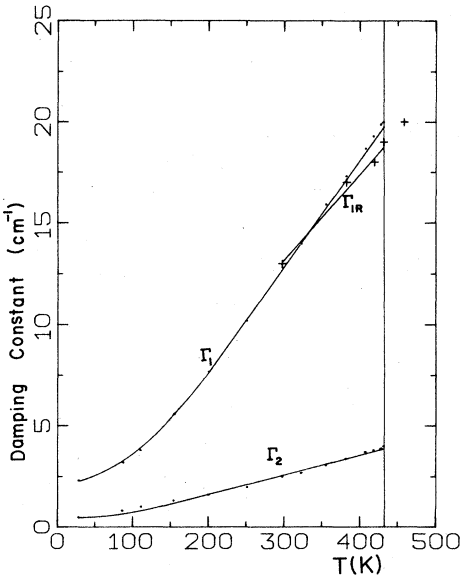

FIG. 10. Temperature dependence of the damping of the bare modes. The meaning of the symbols is explained in the text.

central mode were present. While the bare frequencies ν_1 and ν_2 cross just below T_{tr}, the coupling δ_{12} between both modes is very strong so that the observed Raman frequencies are strongly repelled from one another. This mode repulsion, due to the magnitude of δ_{12}, is present, though less marked, at all temperatures. Also, the fact that both peaks are of comparable strength has the same origin. The temperature dependence of the squares of the soft-mode frequencies Ω_{IR}^2 and Ω_R^2 is strongly nonlinear, leading to instability just above T_{tr}. This means that the critical exponent γ for the static susceptibility, which is proportional to Ω^{-2}, is greater than 1. (It should be stressed that, theoretically, the temperature dependence of Ω_{IR} and Ω_R must be the same, even if their magnitudes are markedly different due to the different models used.) This is apparently not a symptom of critical behavior. Similar deviations are seen in measurements of P_s, shear strain, birefringence,[21] and in the Bragg intensities of superlattice reflections determined by elastic neutron scattering,[1] all of which should be proportional to η_s^2 but show obvious nonlinearity. This behavior was fully explained by using the classical thermodynamical theory including sixth-order terms in the free-energy expansion.[1] We have not tried to fit the behavior of $\Omega^{-2}(T)$ by thermodynamic theory, because the accuracy of our data close to T_{tr} is insufficient. However, an easier check on the internal consistency of our results could be provided by comparison with the observed anomaly in the elastic constant C_{11} and in the clamped permittivity ϵ_c. This is discussed later.

In Fig. 10 the temperature dependence of the damping constants is shown. As discussed earlier, the Raman line dampings are not the result of unconstrained least-squares fitting. The fact that the infrared damping nearly coincides with Γ_1 is presumably accidental because the bare infrared soft mode is not identical to the Q_1 Raman mode.

In Fig. 11 the temperature dependence of the coupling constants between the soft modes and the central peak is shown. Our best fit was obtained with δ_{13} temperature independent, while δ_{23} and δ from infrared data show similar pronounced increases near T_{tr}. This means that a nonlinear increase in the coupling between the bare Raman-inactive hard mode at 59 cm^{-1} and the central

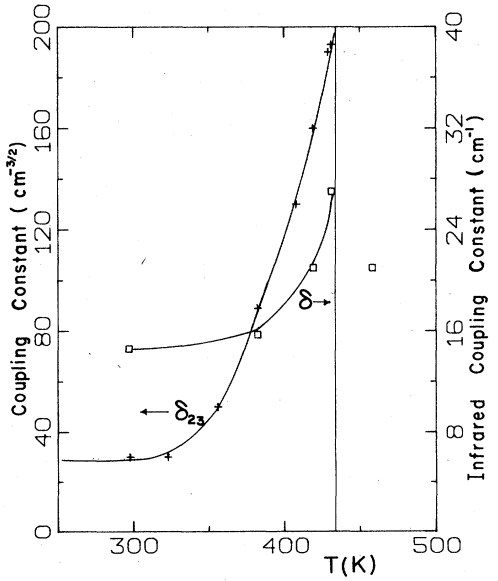

FIG. 11. Temperature dependence of the coupling between the soft and central mode. The coupling constant $\delta_{13} = -50\ cm^{-3/2}$ is temperature independent. The meaning of the symbols is explained in the text.

peak is the main cause for the occurrence of a phase transition as T_{tr} is approached from below. The other two subsidiary causes are the temperature dependence of ν_1 and the strong (temperature-independent) coupling between the Q_1 and Q_2 modes.

Thus the following picture of the dynamical origin of the phase transition in GMO emerges: As T_{tr} is approached from below, the Raman-active bare mode Q_1 is temperature dependent and softens to zero at a temperature ~ 850 K. This mode is strongly coupled to a Raman-inactive hard mode at 59 cm^{-1}. This coupling decreases the critical temperature to ~ 550 K and, near T_{tr}, the new soft mode consists of an equal admixture of both Q_1 and Q_2 displacements. Both components are coupled to the central mode Q_3, but the coupling to the Q_2 mode dominates near T_{tr}. This further reduces the instability temperature to $T_c' = 435$ K and the ultimate soft mode consists of a mixture of all the coordinates, Q_1, Q_2, and Q_3, which interacts with totally symmetric acoustic modes. This last coupling produces partial softening of the corresponding elastic constants, but the coupling constant decreases to zero at T_c' due to symmetry, since above T_{tr} the soft modes go to the M point. Thus this coupling does not influence the final instability temperature.

An important check on the internal consistency of our results, as was alluded to previously, as well as a further test of our model, is to attempt to explain quantitatively the anomaly in $C_{11}(T)$. According to the detailed thermodynamic analysis by Yao *et al.*[19] and Fleury *et al.*,[16] below T_{tr} this elastic constant is given by

$$C_{11}(T) = C_{11}^0 - \frac{B\eta_s^2(T)}{\Omega^2(T)} . \tag{18}$$

Here C_{11}^0 is the elastic constant in the parent phase or, more accurately, the value obtained by linear extrapolation from high temperature to T_{tr}. B depends both on the coupling between the order parameter and the strain and on the phase of the complex order parameter; it is assumed to be temperature independent. Ω is the effective soft-mode frequency probed by acoustic experiments and is identical to Ω_{IR} and Ω_R because the acoustic frequencies are much lower than the central-mode relaxation frequency, ν_3. Equation (18) has been simplified to include only one soft mode because the splitting is negligible above 300 K. In Fig. 12 we show the experimental curve for $C_{11}(T)$ measured by Höchli,[23] together with the anomalies predicted by our analysis of the infrared and Raman data. Again, it was assumed that $n_s(T) \propto P_s$.[21] Both curves from our analysis were adjusted to fit the acoustic anomaly at 298 K. One can see that the agreement with the infrared and Raman data is satisfactory. Essentially, both predicted curves show clearly the pronounced decrease of C_{11} near T_{tr}. Examination of Eq. (18) shows clearly the basic origin of the anomaly: Both Ω_{IR} and Ω_R decrease faster than P_s close to T_{tr}. This enhanced softening is produced by the sharp increase in coupling between the Q_2 mode and the central mode. If one replaces the frequency Ω_R by the directly observed Raman frequency ν_-, as was frequently done in the past,

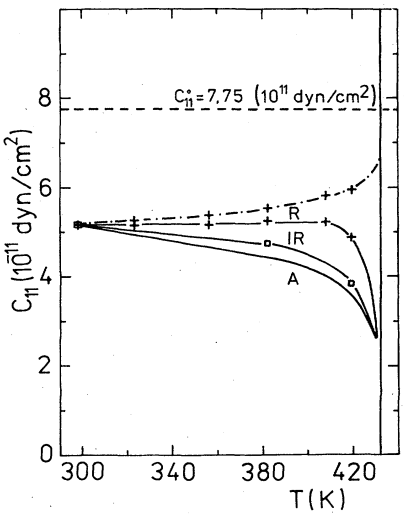

FIG. 12. Temperature dependence of the C_{11} elastic anomaly. Curve A is after the ultrasonic data of Hochli (Ref. 23); curves R and IR are results derived from our Raman and infrared data, respectively. The dashed-dotted curve is calculated with the observed Raman soft-mode frequency ν_-. All curves are normalized to fit the ultrasonic value at 300 K.

a qualitative disagreement with the acoustic experiment is observed (see the dashed-dotted line in Fig. 12.). The slight difference in the rates at which Ω_{IR} and Ω_R soften, which produces the difference between the IR and R lines in Fig. 12, is within the limit of uncertainty of our fits. In this context, one should also bear in mind that C_{11}^0 and B can be slightly temperature dependent and that the relation $P_s \propto \eta_s^2$ is only strictly valid close to T_{tr}. Thus the use of Eq. (18) over a temperature range of 135 K is of questionable validity.

Our model can also be used to estimate the acoustic-mode damping which is known from Brillouin scattering[16] and ultrasonic attenuation.[24,25] However, an accurate calculation near T_{tr} requires a knowledge of the entire soft branches in $\vec{k}$ space, including the central-peak dispersion. Therefore we have not attempted to calculate this effect, but we observe that approximate calculations by others[24,25] of the ultrasonic attenuations for longitudinal waves propagating along x and y crystallographic directions lead to large differences in estimated central-mode widths (i.e., the dressed relaxation frequency). Courdille *et al.*[24] obtained only 0.8 cm^{-1} for TMO at 413 K, whereas Esayan *et al.*[25] derived 5.3 cm^{-1} for GMO at the same temperature. The latter is much closer to our result (~ 8 cm^{-1}; see Figs. 7 and 8).

Another important test of our model is the anomaly in the clamped permittivity shown in Fig. 6. Equation (10) gives the contribution of the soft and central modes to the clamped static permittivity in a simple form

$$\Delta\epsilon_s(0) = \frac{f_{IR}}{\Omega_{IR}^2} . \tag{19}$$

The total clamped permittivity is given by

$$\epsilon_c = \Delta\epsilon_s(0) + \epsilon_\infty , \tag{20}$$

where ϵ_∞ is the contribution of all higher-frequency modes. In Fig. 6 the values of ϵ_c following from the dielectric fit in Table I are shown under the assumption that ϵ_∞ is independent of temperature and ϵ_c fits the experimental value at 294 K. The agreement is very good and, below T_{tr}, completely within the limits of error of our fit. This anomaly is so weak (~ 1–2%) and easily obscured that earlier data[26] apparently did not reveal its presence. The slight disagreement above T_{tr} is probably caused by a weak temperature dependence of ϵ_∞.

Our model predicts weak central-peak singularities at T_{tr} in both dielectric loss ϵ'' and light scattering spectra. Our experimental data on ϵ'' clearly show that the former singularity exists. With regard to the latter, the situation is ambiguous. In earlier work[14,15] this singularity was observed, in good quantitative agreement with our model, in contrast with more recent work[16] which reports no such behavior. However, Fig. 2 of Ref. 16, which shows the low-frequency part of $x(zz)y$ Raman spectra in TMO, seems to be in qualitative agreement with our model. Also our model is in qualitative agreement with inelastic neutron scattering data on TMO,[1] which show an incompletely resolved central peak below T_{tr}. In addition, neutron scattering data[1] also show the appearance of a hard T_1-symmetry mode at the M point at ~ 62 cm^{-1} (7.7 meV) above T_{tr}. This frequency is slightly higher than our bare ν_2 frequency below T_{tr}. This can be understood as the result of coupling with the soft mode which, above T_{tr}, lies at a much lower frequency. It is thus natural to connect this mode to the hard ν_2 doublet below T_{tr}.

Finally the important question arises as to the microscopic origin of the central mode. First, we notice that the central-mode width found in GMO is the highest ever observed. This argues for its intrinsic nature, rather than for the influence of defects. Moreover, there is no evidence that the central-mode spectra are strongly dependent on the sample quality. Among intrinsic central-mode mechanisms, that based on weak anharmonic coupling to phonon-density fluctuations[27] predicts a decrease of the coupling constants to zero at T_{tr}. It cannot therefore explain the increase of coupling near T_{tr}. This argues in favor of those mechanisms based on strong anharmonicity and probably for a partial disorder near T_{tr}. It is also worth noting that there is good evidence for the existence of central peaks in the (1–10)-cm^{-1} region from dielectric measurements on several displacive *proper* ferroelectrics: e.g., $BaTiO_3$, $KNbO_3$, $LiTaO_3$, $LiNbO_3$, and SbSI.[28] However, this evidence is so far mostly qualitative so that no quantitative comparison with our results is possible. Our results differ strongly from those obtained by light and neutron scattering studies on other systems: e.g., $SrTiO_3$, $Pb_3Ge_3O_{11}$, KH_2PO_4, and $BaMnF_4$.[27,29,30] These generally show much narrower central peaks, with widths of the order of 1 cm^{-1} or less, which appear to be markedly influenced by defects.

V. CONCLUSIONS

In this work, we have found from dielectric measurements in the (5–50)-cm^{-1} region direct evidence for the existence of an overdamped central mode in GMO with a bare relaxation frequency near 20 cm^{-1}. The softening of the infrared-active soft mode is weak, but its coupling to the central mode increases close to T_{tr}, producing instability just above T_{tr}. This behavior accounts well for the weak anomaly in the clamped permittivity and was confirmed independently and made more precise by a new and comprehensive analysis of earlier Raman scattering data which invokes coupling of Raman modes to the central mode. It was found that two underdamped doublets are involved in the transition. These are strongly coupled both to one another and to the overdamped central mode. Neglecting the doublet nature of these modes, a three-coupled-mode analysis has shown that the bare modes have the following basic features: The highest mode carries the entire Raman strength and softens (roughly classically). It is strongly coupled to a Raman-inactive hard mode at 59 cm^{-1} and to a central mode with a relaxation frequency of 20 cm^{-1}. Both coupling constants are temperature independent. The lower-frequency hard mode is also coupled to the central mode, but with increasing coupling constant close to T_{tr}. Whereas the parameters of both underdamped modes are reliably established from the fit between 28 K and T_{tr}, the parameters of the central peak, including its coupling to both underdamped modes, can only be reliably determined above 300 K.

In this way, we have developed a phenomenological model of the dynamical behavior of GMO in the ferroelectric phase whose predictions appear to be in satisfactory agreement with reported experimental data. The central-mode width in GMO is higher than that found for any other crystal showing a structural phase transition. We believe this feature to indicate the intrinsic nature of the central mode and the presence of partial disorder near T_{tr}.

ACKNOWLEDGMENTS

A critical reading of this manuscript by V. Dvořák is gratefully acknowledged. Work at the University of Nebraska was supported by the U. S. Army Research Office.

[1] B. Dorner, J. D. Axe, and G. Shirane, Phys. Rev. B **6**, 1950 (1972).
[2] J. Petzelt and V. Dvořák, Phys. Status Solidi B **46**, 413 (1971).
[3] V. Dvořák and J. Petzelt, Phys. Lett. **35A**, 209 (1971).
[4] J. Petzelt and V. Dvořák, J. Phys. C **9**, 1587 (1976).
[5] P. A. Fleury, Solid State Commun. **8**, 601 (1970).
[6] F. G. Ullman, B. J. Holden, B. N. Ganguly, and J. R. Hardy, Phys. Rev. B **8**, 2991 (1973).
[7] B. N. Ganguly, F. G. Ullman, R. D. Kirby, and J. R. Hardy, Solid State Commun. **17**, 553 (1975).
[8] B. N. Ganguly, F. G. Ullman, R. D. Kirby, and J. R. Hardy, Phys. Rev. B **13**, 1344 (1976).
[9] T. Shigenari, Y. Takagi, and V. Wakabayashi, Solid State Commun. **18**, 1271 (1976).

[10]Y. Takagi, Y. Wakabayashi, and T. Shigenari, J. Phys. Soc. Jpn. **41**, 719 (1976).
[11]B. N. Ganguly, F. G. Ullman, R. D. Kirby, and J. R. Hardy, J. Phys. Soc. Jpn. **43**, 1085 (1977).
[12]Q. Kim and F. G. Ullman, Phys. Rev. B **18**, 3579 (1978).
[13]R. Laiho, S. D. Prokhorova, I. G. Siny, E. G. Kuzminov, V. D. Mikvabia, and T. M. Polkhovskaya, Ferroelectrics **21**, 339 (1978).
[14]I. G. Siny, S. D. Prokhorova, E. G. Kuzminov, V. D. Mikvabia, and T. M. Polkhovskaya, Izv. Akad. Nauk. SSSR **43**, 1658 (1979).
[15]G. A. Smolensky, I. G. Siny, S. D. Prokhorova, E. G. Kuzminov, and V. D. Mikvabia, J. Phys. Soc. Jpn. Suppl. B **49**, 26 (1980).
[16]P. A. Fleury, K. B. Lyons, and R. S. Katiyar, Phys. Rev. B **26**, 6397 (1982).
[17]J. Petzelt, Solid State Commun. **9**, 1485 (1971).
[18]P. A. Fleury and K. B. Lyons, in *Structural Phase Transitions I,* Vol. 23 of *Topics in Current Physics,* edited by K. A. Müller and H. Thomas (Springer, Berlin, 1981), pp. 9–92.
[19]W. Yao, H. Z. Cummins, and R. H. Bruce, Phys. Rev. B **24**, 424 (1981).
[20]A. A. Volkov, G. V. Kozlov, and S. P. Lebedev, Zh. Eksp. Teor. Fiz. **79**, 1430 (1980).
[21]S. E. Cummins, Ferroelectrics **1**, 11 (1970).
[22]J. Feder, in *Local Properties at Phase Transitions,* edtied by K. A. Müller and A. Rigemonti (North Holland, Amsterdam, 1976), pp. 312–332.
[23]U. T. Höchli, Phys. Rev. B **6**, 1814 (1972).
[24]J. M. Courdille, R. Deroche, and J. Dumas, J. Phys. **36**, 891 (1975).
[25]S. K. Esayan, B. D. Laykhtman, and V. V. Lemanov, Zh. Eksp. Teor. Fiz. **68**, 689 (1975).
[26]L. E. Cross, A. Fouskova, and S. E. Cummins, Phys. Rev. Lett. **21**, 812 (1968).
[27]A. D. Bruce and R. A. Cowley, Adv. Phys. **29**, 219 (1980).
[28]J. Petzelt and V. Dvořák, in *Vibrational Spectroscopy of Phase Transitions,* edited by F. Owens and Z. Iqbal (Academic, New York, 1984).
[29]D. W. Bechtle, J. F. Scott, and D. J. Lockwood, Phys. Rev. B **18**, 6213 (1978).
[30]K. B. Lyons, Ferroelectrics **35**, 37 (1981).